

A Survey of Eclipsing Binary Stars in the Eastern Spiral Arm of M31

Ian Todd^{1*}, Don Pollacco¹, Ian Skillen², D.M. Bramich³, Steve Bell⁴ and Thomas Augusteijn⁵

¹*APS Division, Department of Physics and Astronomy, Queen's University of Belfast, Belfast, BT7 1NN, UK*

²*Isaac Newton Group of Telescopes, Apartado 321, E-38700 Santa Cruz de La Palma, Tenerife, Spain*

³*Department of Physics and Astronomy, University of St Andrews, North Haugh, Fife, KY16 9SS, UK*

⁴*HM Nautical Almanac Office, CCLRC Rutherford Appleton Laboratory, Chilton, Didcot, Oxon., OX11 0QX, UK*

⁵*Nordic Optical Telescope, Apartado 474, E-38700 Santa Cruz de La Palma, Tenerife, Spain*

Accepted ?????. Received ????; in original form ?????

ABSTRACT

Results of an archival survey are presented using *B*-band imaging of the eastern spiral arm of M31. Focusing on the eclipsing binary star population, a matched-filter technique has been used to identify 280 binary systems. Of these, 127 systems (98 of which are newly discovered) have sufficient phase coverage to allow accurate orbital periods to be determined. At least nine of these binaries are detached systems which could, in principle, be used for distance determination. The light curves of the detached and other selected systems are presented along with a discussion of some of the more interesting binaries. The impact of unresolved stellar blends on these light curves is considered.

Key words: binaries: eclipsing, galaxies: Local Group, galaxies: M31

1 INTRODUCTION

The determination of accurate distances to the galaxies of the Local Group is of fundamental importance in several areas of modern astronomy. These galaxies serve as a natural laboratory for studies of stellar formation and evolution over a wide range of physical environments. A knowledge of their distances permits the determination of the intrinsic physical properties of their resolved stellar content and provides an insight into population synthesis modelling of the formation and evolution of galaxies. Furthermore, the Local Group galaxies provide a critical step in determining the cosmological distance scale by calibrating standard candles such as Cepheids, extending the distance ladder to galaxies far beyond the Local Group. This leads to a determination of the Hubble Constant and the age of the universe. Recent results, primarily from the Distance Scale Key Project (Freedman et al. 2001; Mould et al. 2004), have led to considerable progress in this field and H_0 is now believed to be known to a precision of 10 per cent. At this level, the uncertainty is dominated by two systematic effects – the absolute distance to the LMC (the first step in the extragalactic distance scale) and the possible dependence of the Cepheid Period-Luminosity relationship on metallicity.

Detached eclipsing binary stars (EBs) offer the possibility of determining the *absolute* properties of a stellar system such as masses and radii. Kaluzny et al. (1998) have suggested that observations of detached EBs can be used to determine accurate absolute luminosities and hence their distance to better than 5 per cent and possibly even 1 per cent; see also Andersen (1991); Clausen (2004). As these distances are based mainly on geometrical arguments with only limited physical input they are often considered to be amongst the most reliable. Hence, distances derived from EBs can be used to calibrate the Cepheid period-luminosity relationship. More recently it has been proposed by Wilson (2004) that semi-detached systems could be used (possibly in preference to detached systems) to the same end. While light curves from these systems may appear more complicated, the physical processes underlying the variations (*e.g.* irradiation and tidal effects) are now well understood.

Gaposhkin (1968) first suggested that EBs could be used to determine distances to the Magellanic Clouds (MCs). In fact in recent years it has become clear that distances derived from EBs can give distances at least comparable to that obtained from the Cepheid period-luminosity relationship. For example, Harries et al. (2003) and Hilditch et al. (2005) have studied 50 SMC binaries and derived a distance of 60.6 kpc with an uncertainty of ~ 5 per cent. Including results from other, equally reliable, surveys

* E-mail: I.Todd@qub.ac.uk

of SMC binaries lead to an overall dispersion in results of ~ 10 per cent which is most likely due to depth effects in this galaxy.

Beyond the MCs, the Andromeda Galaxy, M31, is an important distance scale calibrator. It does not suffer from the extreme metallicities of the MCs and, being a spiral galaxy, its geometry is far better understood than that of the irregular MCs. This galaxy is also a fundamental calibrator of the zero-points of the planetary nebula and globular cluster luminosity functions, and is the first step of the Tully-Fisher relationship for spiral galaxies. Consequently, M31 is a more appropriate Local Group standard calibrator than the LMC (Clementini et al. 2001). However, recent distance estimates for M31 based on Cepheids and the brightness of the tip of the red giant branch (*e.g.*, (McConnachie et al. 2005; Freedman et al. 2001)) show discrepancies at the ~ 10 per cent level.

There have been several surveys of M31 specifically to detect variable stars. For example, Baade & Swope (1963) used photographic plates to identify 684 variables in four fields, ~ 58 per cent of which were Cepheids and a further 9 per cent EBs. Currently, a total of around 300 binaries are known from various surveys (Guinan 2004).

The DIRECT Project (Kaluzny et al. 1998) has been attempting to derive distances to M31 and M33 from EBs with sufficient accuracy to calibrate the Cepheid distances. Using 1.0-m telescopes they have discovered a total of ~ 130 EBs in both galaxies.

In this paper, we present the results of an analysis of archival images obtained over a three year baseline and centred on the eastern arm of M31. We use these data to identify eclipsing systems, with an emphasis on those suited to detailed follow-up and distance determination.

2 OBSERVATIONS AND DATA REDUCTION

The data forming the basis of this study were obtained over the period 2000-2003 by scheduled observers on the 2.5-m Isaac Newton Telescope (INT) on the Island of La Palma in the Canary Islands. These data were retrieved from the Isaac Newton Group of Telescopes (ING) Archive located at CASU, University of Cambridge.¹

The INT is equipped with a Wide Field Camera (WFC) comprising four 4096×2048 EEV42 detectors. The $f/3.3$ prime focus of the INT has a plate scale of 0.33 arcsec pixel⁻¹ on the CCD and the camera has a relatively unvignetted field of ~ 1000 arcmin² across the four chips. Data were obtained in weekly runs, scheduled in September or October of each year. *BV* exposures were made at approximately alternate intervals; around 200 images in *B* and 169 in *V* were taken, with exposure times of 900s in each filter. The data used here were obtained in median seeing better than 1.3 arcsec, and a summary of the images used is given in Table 1. The observed fields approximately coincide with those of the DIRECT Project (fields A – D) and the fields of Magnier (1996) in the rich eastern spiral arm. The data are well sampled on short timescales, but are less well sam-

Table 1. Summary of observation log. The precise number of observations for each star will vary depending on the quality of its point spread function on that particular image, *e.g.* being near the edge of, or near a bad column on the CCD.

Year	# B Images	# V Images	HJD Range 2,450,000+	Median Image Quality (arcsec)
2000	32	30	1811.5 – 1814.5	0.99
2001	35	37	2200.4 – 2206.5	1.20
2002	52	18	2546.4 – 2550.5	1.30
2003	81	84	2906.4 – 2910.7	0.97

Table 2. Linearity Correction Coefficients for IRLINCOR

CCD #	c_1	c_2	c_3
1	1.0	-0.081918	0.012884
2	1.0	-0.0016384	-0.0042947
3	1.0	-0.019660	0.0
4	1.0	-0.0049151	-0.0021474

pled for the intermediate periods of 4-10 d which are typical of massive, detached binaries.

2.1 Data reduction

Each of the four fields comprising the WFC was analysed individually. Reduction to science frames proceeded automatically using the IRAF² data reduction package and a series of scripts. The master bias frame was created from all biases and subtracted from all flats and science frames, and a linearity correction was applied with IRLINCOR, using cubic linearity correction. Coefficients obtained from the INT Wide Field Survey website³ are listed in Table 2. Master flats for each filter were created with appropriate bad pixel and cosmic ray rejections, and the raw object frames were reduced to science frames with CCDPROC.

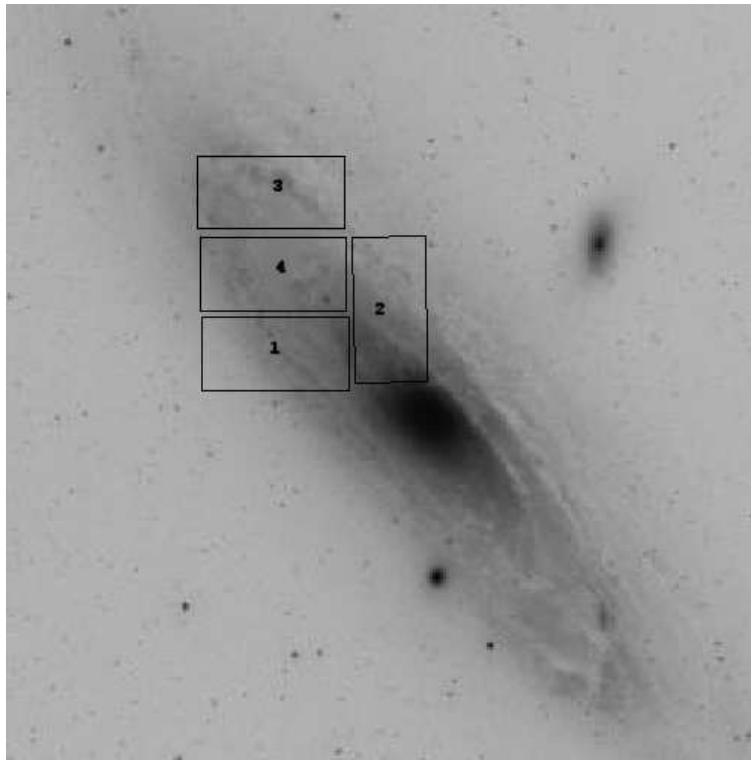
2.2 Image Difference analysis

Lightcurves were derived from the science frame using difference image analysis (DIA). The software used in this study has been described in Bond et al. (2001) and Bramich et al. (2005), hereafter BBDA. DIA attempts to match the point spread function (PSF) between the frames in a time sequence by generating a best seeing reference frame and then degrading that reference frame to the seeing of the individual frames of the observing run. The empirically-generated kernel solution models the changes to the PSF from one image to another; it is solved for each image – reference pair. Non-varying stars leave no residual on the difference image, and variables leave either positive or negative flux with respect to the reference frame. The flux is compared with the

¹ ING archive at <http://archive.ast.cam.ac.uk>

² IRAF is written and supported by the IRAF programming group at the National Optical Astronomy Observatories (NOAO) in Tucson, Arizona. NOAO is operated by the Association of Universities for Research in Astronomy (AURA), Inc. under cooperative agreement with the National Science Foundation

³ <http://www.ast.cam.ac.uk/~wfsur/technical/ccd/>

Figure 1. The four WFC fields surveyed in this study superimposed on a DSS2 image.

reference frame and converted to magnitudes to generate light curves. DIA is *essential* in crowded fields such as M31, where the high stellar density makes aperture photometry inadequate, and varying backgrounds make PSF modelling alone difficult. An overview of the procedure is given here, however, a more detailed description can be found in BB-DIA.

2.2.1 Photometry

The reduced science frames were passed into the image subtraction pipeline for reference frame generation, subtraction and photometry.

Reference frame generation was performed by selecting several frames with optimal seeing and aligning and stacking them to increase signal to noise. Around 12 frames were chosen to create the reference frame, all with a FWHM of less than 1 arcsec. Each science frame was aligned to the reference frame and subtracted according to

$$Diff(x, y) = I(x, y) - Ref(x, y) \otimes Ker(u, v) - Bg(x, y) \quad (1)$$

where $Diff(x, y)$ is the difference image, $I(x, y)$ is any image in the time series, $Ker(u, v)$ is the kernel that matches the image and reference PSF, $Ref(x, y)$ is the reference frame and $Bg(x, y)$ is the spatially varying differential background. The remaining frame consists of Poisson noise and the residuals of varying objects. Photometry can then be performed on each residual flux to determine how it changes from frame-to-frame. An IDL⁴ script then converted this

flux to magnitudes relative to the stacked reference frame according to equations 2 and 3 (from BB-DIA).

$$f_{tot}(t) = f_{ref} + \frac{f_{diff}(t)}{p(t)} \quad (2)$$

$$m(t) = 25.0 - 2.5 \log(f_{tot}(t)) \quad (3)$$

The total flux, f_{tot} , from a star at time t represents the combination of reference flux f_{ref} and difference flux f_{diff} . The photometric scale factor $p(t)$ takes into account the change in extinction and exposure time from frame to frame. Uncertainties in all flux measurements are propagated accordingly. RMS diagrams for field A are shown in Figure 2, and demonstrate a photometric accuracy of better than 1 per cent for objects as faint as 21st magnitude.

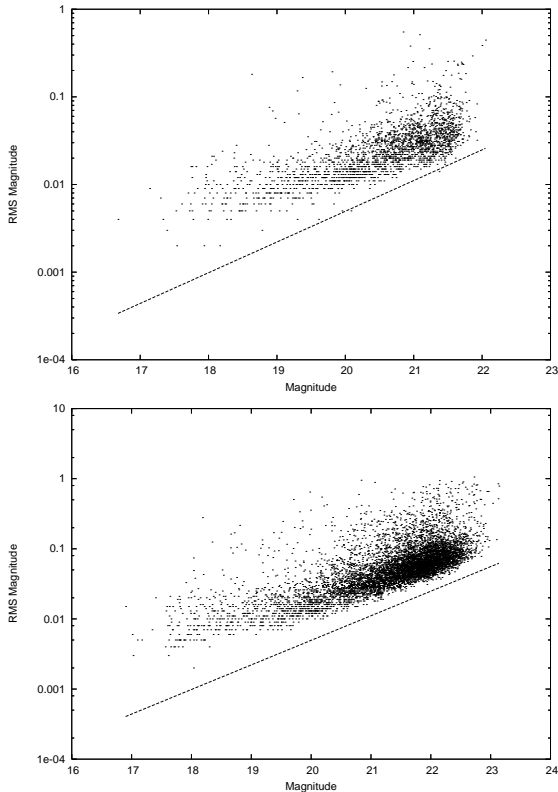
The instrumental magnitudes were then mapped to the Magnier (1996) or Mochejska et al. (2001) dataset via a linear transformation using the stars found on the reference frame and solved for using a least squares process. Unresolved stellar blends can affect the absolute magnitude and amplitude calibrations. The impact of such blends on the light curves is discussed in more detail in Section 3.

2.2.2 Astrometry

The astrometric solution was calculated for the frame using tasks from the IRAF package IMCOORDS. Once again, the dataset used for reference frame was that of Magnier (1996). Ten widely-spaced stars on the frame were used as a starting point for the astrometric solution, followed by the use of automated scripts to correlate positions of bright stars

⁴ IDL provided, under license, by Research Systems Inc.

Figure 2. RMS diagrams for CCD#1 of field A. Filters are *B* (top) and *V* (bottom) respectively. The theoretical line is from SIGNAL, available from the ING. At the faint end of the observations the elevation above the theoretical line is due to the sky brightness from unresolved background stars. At the bright end the deviation is caused by inadequacies in the model. The unusual “bump” between magnitudes 22 and 23 should be noted for the *V* filter data. This is may be caused by DIA attempting to simulate the very faint and highly-crowded background stars. As no EBs are identified at this magnitude, it is of no relevance to this study but is worthy of note.



with entries in the USNO-B1.0⁵ catalogue. This procedure quantifies the pin-cushion distortion present on the WFC; typical differences were approximately 0.4 arcsec RMS, due to a combination of the CCD distortion and that introduced in constructing the reference frame.

The plate solution was then calculated for all the variables, converting frame positions to J2000.0 celestial coordinates in the equatorial system based on the astrometric solution.

2.2.3 Variability detection

Since DIA only selects the stars that are variable, the detection of variability is not an issue. However, the level of variability is important so as to remove light curves that have low intrinsic variability and high photometric error. An implementation of the Stetson Variability Index (SVI),

based on that adopted by Kaluzny et al. (1998), was employed to detect high amplitude stars with low errors. The index is given by

$$J = \frac{\sum_{k=1}^n w_k \operatorname{sgn}(P_k) \sqrt{P_k}}{\sum_{k=1}^n w_k} \quad (4)$$

where k pairs of observations are defined, each with weight w_k . The value P_k is defined as the product of normalized residuals of the paired observations i and j :

$$P_k = \begin{cases} \delta_{i(k)} \delta_{j(k)}, & \text{if } i(k) \neq j(k) \\ \delta_{i(k)}^2 - 1, & \text{if } i(k) = j(k) \end{cases}$$

Finally δ is the magnitude residual of a given observation from the mean, given over n observations in a passband by

$$\delta = \sqrt{\frac{n}{n-1} \frac{\nu - \bar{\nu}}{\sum \nu}} \quad (5)$$

where ν is the magnitude. J should tend to zero for a non-variable star and be positive for a variable. Observations i and j will be in different pass bands at (approximately) the same epoch. If only one observation is made at a particular epoch, $i(k) = j(k)$.

In determining the variability index, the maximum time separation in the same filter for two measurements to be considered a pair was around 90 minutes. If two points were a pair then the weight given was 1.0, otherwise 0.25.

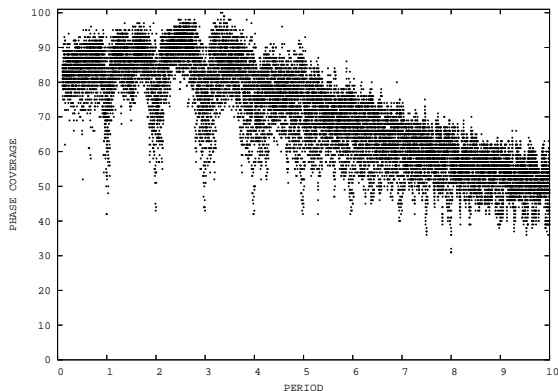
2.3 Matched Filters

Classification of the variable stars was performed automatically by matching theoretical curves to the observed folded light curve by least squares fit. Two simple classifying light curves were chosen; EB and Cepheid. The classification code sampled multiple parameter space in terms of period and light curve shape, varying the amplitude and depth of eclipses, and searched for periods the range 0.5 to 15 d. Secondary eclipse amplitudes adopted lay in the range 0.3 to 0.9 magnitudes and assumed to be at phase 0.5 (i.e. circular orbits). Primary eclipse amplitudes were scaled to the amplitude of the light curve. This allowed broad classification to be made but in many cases light curves were mis-identified due to sparse sampling. Some binaries were missed because the light curves had higher than normal scatter or several outlying observations distorted the χ^2 fit.

To resolve this, a simple code was written that searched each light curve in the time domain for linear trends, subject to various gradients and fit coefficients. This is a similar approach to the ‘box-fitting’ technique used to search for the short eclipses of extrasolar planets. This particular approach could not be used here because the light curves are not continuously sampled over the eclipses. Instead, searches for the ‘characteristic fragments’ of an EB were made – sharp, almost linear, ascents and descents around eclipse. This revealed at least twice as many EBs as the simple matched filter algorithm, but also revealed many false positives, such as Cepheids. All light curves classified as EBs were inspected by eye to validate their classification, with rejection of those that were not believed to be binaries.

⁵ Provided by United States Naval Observatory, Washington D.C.

Figure 3. Simulation of orbital phase coverage for our dataset. The phase space $[0, 1]$ is divided into 100 equal bins. A dataset with at least one point in each bin is said to have 100 per cent phase coverage.



2.4 Period Determination

Period finding in these sparse time series was difficult. Various methods such as PDM (Stellingworth 1978), ANOVA due to Schwarzenberg-Czerny (1989) and various string length techniques were tried; in general PDM gave more consistent results. A visual inspection code was also drawn up, whereupon a period was specified and the light curve folded appropriately. In cases where automated period-finding techniques failed to give reliable results, variable incremental shifts in period were applied and the folded light curve was inspected in real-time by eye. The major difficulty in the period determination is aliasing. Due to the sampling of the data induced by the observational constraints, some of the fainter and noisier light curves have several PDM peaks. In cases where the true peak could not be identified, it is impossible to say for certain whether the selected period is *definitely* the correct one without additional data, only that it is close; such cases have been noted in the tables. Ambiguity can also arise when limited phase coverage prevents both primary and secondary minima from being detected; a phase coverage simulation for this dataset is shown in Figure 3.

2.5 Results

The EBs identified in our analysis, with periods (where available) are listed in Tables 3, 4, 5 and 6. In these tables, objects with significant aliasing issues are annotated with their corresponding periods. Difference fluxes are an estimation of the depth of the primary and secondary eclipses in ADU/s, but in many cases the deepest part of the eclipses were not sampled by our data. Quadrature magnitudes are listed, but because of the likelihood of stellar blends affecting many objects on the reference frame, the presented magnitudes are likely to be unreliable.

Attempts have been made to match this catalogue with those of others, in particular, the DIRECT Project and in some cases those of Berkhuijsen et al. (1988), hereafter BHGZ88. Detached eclipsing binaries (DEB) detected in this study and by the DIRECT Project are noted.

3 DISCUSSION

The matched filter analysis detected many objects with fragments of light curves that are consistent with that of an eclipsing binary. In cases where sufficient data were available to determine periods, attempts were made to rule out aliases by searching for periods in subsets of the data to determine consistency in the power spectra, and by randomizing the brightness measurements on the time axis to derive significance contours.

The DIRECT Project found 34 EBs coincident with the observed field, and the observations tabulated in this study have recovered all but 5 of these. The undetected objects are all long period systems, objects for which this study is not expected to be sensitive (see Fig. 3). Of particular interest are two objects, V6105B and V888B, classified as detached systems by DIRECT. Both of these objects have been recovered and their detached nature confirmed. In principle, these objects could be used for accurate distance determinations, and DIRECT considers them suitable systems for detailed follow-up both photometrically and spectroscopically (Macri 2004).

Other noteworthy systems include:

f4BEB1802. This is a short period system ($P=0.232$ d), originally discovered by DIRECT (# V438). Its brightness and colour suggest it is a foreground object. The photometry presented here does not constrain the period well due to its high scatter when phased, indicating long-term intrinsic variability.

f1BEB1205, *f1BEB1448* (DIRECT #V10550), *f3BEB456*, and *f4BEB1180* are all bright semi-detached systems.

f3BEB760. This is a bright, long-period detached system, and is ideal for follow-up spectroscopy. *f4BEB1763*, *f1BEB1181*, *f1BEB939* and *f2BEB1850* are also detached systems. The photometry presented here is not of sufficient quality for accurate light curve analyses.

3.1 Blending

Unresolved background stars are believed to be a major cause of elevated background levels in the images studied here; the effect of this problem is demonstrated in Figure 2. It is reasonable to expect that crowding issues will affect the accuracy of the photometry presented here due to a significant proportion of unresolved blended images. This problem of blending is discussed in detail in Kiss & Bedding (2005). *Blending will contribute errors in the absolute flux measurement on the reference image, and hence the quadrature magnitudes and eclipse depths of blended EBs will be incorrect.* It is for this reason that results are presented here in terms of difference flux units, as periods and difference fluxes will be relatively unaffected by blending. The level of blending can be estimated with high resolution imaging by HST and such imaging of systems that are to be used in distance determination is essential.

The median FWHM of the images analysed here, ~ 1 arcsec, corresponds to a spatial resolution of 3.6 pc in M31. Mochejska et al. (2004) have investigated the third light contamination of ground-based photometry of 22 Cepheids in M31 using HST imaging. They find in the *V*-band that, on average, ~ 19 per cent of the stellar flux is caused by a resolvable companion. Given that the physical size of a WFPC2

Table 3. EBs in Field 1 of the Andromeda Galaxy. D_p and D_s are the depth of the primary and secondary eclipses in ADU/s respectively.

ID	RA (J2000)	DEC (J2000)	P (d)	B_{max}	V_{max}	D_p	D_s	Notes
f1BEB1448	0:44:29.272	41:23:01.446	3.1690	19.20	19.28	50	42	V10550 DIRECT
f1BEB1500	0:44:26.974	41:23:42.531	3.3461	21.11	20.97	7.2	4.1	1, V9904 DIRECT
f1BEB1141	0:44:40.021	41:26:49.084	1.2614, 1.2636	21.55	21.74	2.1	0.9	
f1BEB1205	0:44:37.988	41:29:23.819	3.5497	19.17	19.22	56	42	V12650 DIRECT
f1BEB1598	0:44:48.675	41:29:15.557	5.7526	19.25	-	27	27	DEB, V9037 DIRECT
f1BEB2228	0:43:50.771	41:21:51.546	2.1767	20.36	20.34	12	8.5	
f1BEB2065	0:43:59.846	41:21:20.108	2.7559	21.37	21.30	6.2	3.2	
f1BEB2349	0:43:46.653	41:23:01.230	2.3705, 2.3783	20.47	20.55	13	12	
f1BEB294	0:45:00.513	41:31:39.543	5.2495	19.60	19.65	14	13	V6105 DIRECT, DEB?
f1BEB575	0:44:53.782	41:31:11.045	7.00	20.31	20.07	16	14	V4903 DIRECT
f1BEB925	0:44:45.269	41:28:00.336	11.542	18.77	18.68	50	30	V13944 DIRECT
f1BEB716	0:44:50.091	41:28:07.222	2.8724	20.17	20.32	22	11	V14662 DIRECT
f1BEB1260	0:44:36.090	41:29:19.592	2.0429	19.81	19.92	16	11	V12262 DIRECT
f1BEB1854	0:44:12.704	41:31:08.555	1.7461	21.00	21.02	7.5	4.9	
f1BEB1813	0:44:13.710	41:22:07.134	2.7121	20.83	20.78	14	7.2	
f1BEB417	0:44:57.387	41:30:07.021	2.1849	21.24	21.10	8.2	6.2	
f1BEB2188	0:43:51.972	41:23:15.402	2.6264	21.27	21.24	4.5	3.5	
f1BEB1152	0:44:39.373	41:25:59.551	2.1423	20.43	20.55	5.5	5.5	DEB?
f1BEB1215	0:44:37.662	41:29:46.339	2.3009	20.40	20.43	12	10	1, V12594 DIRECT
f1BEB304	0:45:00.121	41:31:09.107	0.8577	21.20	21.28	4.0	3.5	
f1BEB1429	0:44:29.889	41:23:27.589	2.3048	20.34	20.58	17	10.5	V10732 DIRECT
f1BEB1407	0:44:30.758	41:24:09.575	1.8129	20.83	20.78	4.7	1.5	
f1BEB2357	0:43:46.740	41:29:51.666	3.1646	20.61	20.67	11.4	10.4	
f1BEB939	0:44:44.929	41:28:03.327	2.3893	21.17	21.03	6.0	5.0	DEB
f1BEB788	0:44:48.572	41:27:27.870	7.1565, 7.2290	21.02	20.95	4	3	2, V14439 DIRECT
f1BEB467	0:44:56.477	41:30:37.289	2.0145	20.21	20.24	8	8	
f1BEB1310	0:44:33.796	41:25:22.180	1.7353	21.16	21.39	4.3	4.3	
f1BEB1262	0:44:35.768	41:24:41.847	2.6606	21.43	21.38	3	2	
f1BEB989	0:44:43.604	41:26:34.587	1.6294	20.48	20.72	9	9	
f1BEB207	0:45:05.051	41:31:56.579	1.6791	21.42	21.48	2.8	2.8	
f1BEB1491	0:44:27.364	41:24:17.867	7.775	20.62	20.62	8.8	5.0	
f1BEB452	0:44:56.829	41:31:11.271	4.258	20.36	20.26	8.0	8.0	V5443 DIRECT
f1BEB321	0:44:59.345	41:30:45.767	2.6684	20.14	20.06	9.0	8.0	BHGZ88?
f1BEB504	0:44:55.912	41:31:10.929	2.8987	20.30	20.32	6.1	6.0	
f1BEB204	0:45:05.077	41:30:21.867	5.9234	21.37	21.18	-	-	2, DEB
f1BEB732	0:44:49.943	41:28:50.896	3.8839	20.44	20.60	19	10	V14653 DIRECT
f1BEB1748	0:44:16.667	41:24:19.373	3.3574	21.37	21.43	5.8	3.1	
f1BEB1766	0:44:15.946	41:22:09.465	2.0834	21.36	21.40	5.4	3.5	
f1BEB1181	0:44:38.179	41:25:30.335	2.4135	21.26	21.07	5.2	5.2	DEB

¹Multiple aliases within ± 0.05 d of the quoted period.²Eclipse has no bottom, therefore flux depth unreliable

pixel is ~ 0.36 pc in M31, and that a young cluster could be < 0.1 pc in diameter, then clearly the Mochejska et al. (2004) estimate is a lower limit (even without considering issues of binarity). The brightest M31 binaries discussed here have $M_V \sim -5.1$ and therefore must have O-type components. Assuming that a Salpeter IMF is applicable in M31 (Veltchev et al. 2004), one might expect that on average ~ 7 B-stars could fall within a single HST pixel and contribute third light.

The EBs with measured periods form a subset of those objects found. Where light curves were sufficient to indicate a *probable* EB, there were many cases where an estimate of the period was not possible. There are around 160 of these objects spread across the four fields. The level of completeness in detection of the EBs is presumed to be low – many

will not have been detected due to inadequate sampling. Overall, 127 eclipsing binaries have been detected – 98 of which are newly discovered. The matched filter analysis also detected many Cepheids and other long-period variables. A discussion of these results will follow in a subsequent paper.

ACKNOWLEDGEMENTS

The INT is operated on the island of La Palma by the Isaac Newton Group in the Spanish Observatorio del Roque de los Muchachos of the Instituto de Astrofísica de Canarias. The production of this work made use of the CONDOR distributed computing software, the Aladin and Vizier services and the NASA/ADS abstract service.

Figure 4. A selection of *B*-band light curves of interest from the dataset. The flux units are adu/sec in each case.

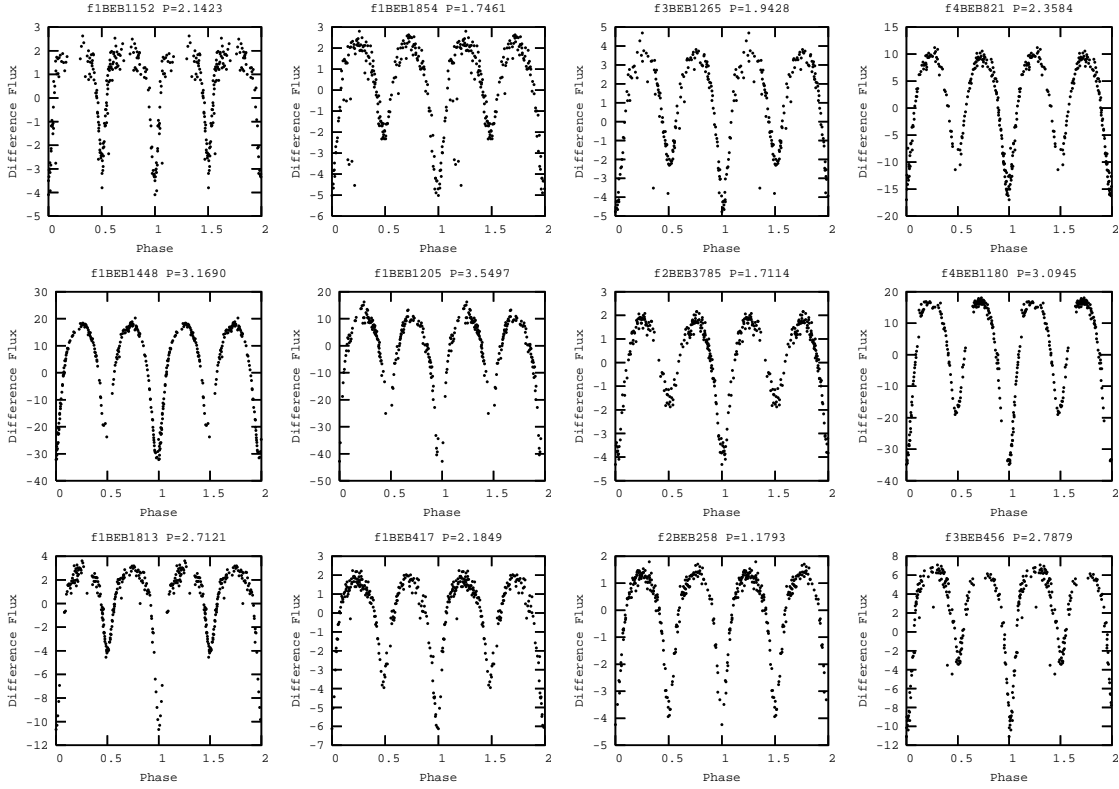


Figure 5. *B*-band light curves of detached EBs. The flux units are adu/sec in each case.

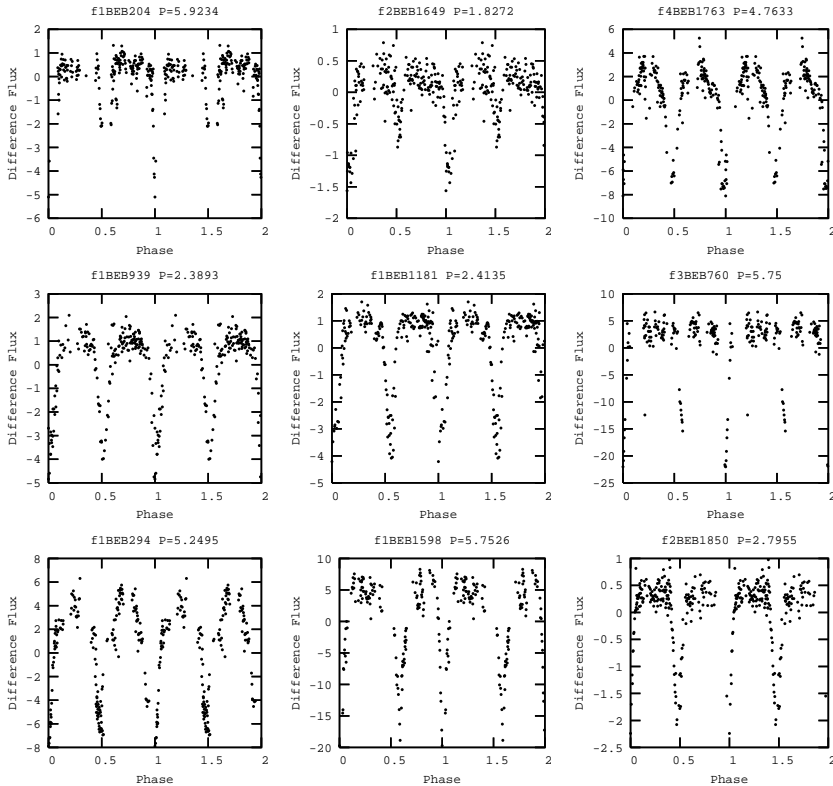


Table 4. EBs in Field 2 of the Andromeda Galaxy.

ID	RA (J2000)	DEC (J2000)	P (d)	B_{max}	V_{max}	D_p	D_s	Notes
f2BEB258	0:43:00.951	41:42:59.781	1.1793	21.24	21.30	5.7	5.5	
f2BEB775	0:42:49.399	41:41:27.051	1.3603	21.22	21.21	3.8	2.7	
f2BEB3137	0:42:47.357	41:32:55.285	0.80186	21.48	21.67	3.2	3.1	
f2BEB450	0:43:29.063	41:42:31.489	1.9751	21.09	20.45	6.25	6.1	Nearby HII region ¹
f2BEB3693	0:43:13.561	41:30:00.140	1.7647	21.75	-	4.5	1.5	
f2BEB1197	0:42:55.767	41:40:12.860	0.83611	20.83	20.88	5.8	5.6	
f2BEB330	0:43:25.453	41:42:50.649	1.1306	21.31	21.52	3.5	3.5	
f2BEB3163	0:43:23.022	41:32:46.434	1.1595	22.10	21.17	2.0	1.7	
f2BEB3695	0:43:31.679	41:29:59.588	1.6121	21.80	21.63	2.4	1.2	
f2BEB563	0:43:06.584	41:42:11.405	3.0198	21.36	21.51	5.4	2.1	
f2BEB1649	0:43:07.370	41:38:39.269	1.8272	22.18	-	1.5	1.0	DEB
f2BEB638	0:42:49.736	41:41:56.432	1.0639	22.94	-	1.1	1.1	
f2BEB5400	0:43:40.511	41:23:05.440	1.3987	21.47	-	2.5	1.5	
f2BEB162	0:43:27.209	41:43:12.934	2.7326	21.92	21.47	1.0	0.8	
f2BEB3785	0:43:38.476	41:29:37.711	1.7114	21.33	21.47	5.8	3.5	
f2BEB5221	0:42:49.977	41:23:37.359	1.8633	20.57	19.58	8.2	3.4	
f2BEB1850	0:43:02.570	41:37:58.881	2.7955	22.33	-	2.6	2.4	DEB
f2BEB2027	0:42:48.376	41:37:25.345	1.5466	21.76	21.83	1.8	1.8	
f2BEB2138	0:42:55.146	41:37:10.325	2.5179, 2.5176	21.76	21.40	2.5	1.7	
f2BEB5325	0:43:40.248	41:23:21.349	3.2248, 3.2535	21.43	21.30	4.7	2.3	
f2BEB2090	0:42:59.898	41:37:17.721	3.5830	20.62	20.53	7.5	3.7	
f2BEB1756	0:42:59.288	41:38:16.991	5.5916	20.37	20.29	11	5.5	
f2BEB3229	0:43:36.559	41:32:29.989	2.022	22.16	21.50	2.0	1.0	
f2BEB630	0:42:46.505	41:41:57.627	5.0963	20.76	20.81	10	3.1	
f2BEB2650	0:42:59.761	41:35:17.018	3.6682	21.04	20.89	3.6	3.6	
f2BEB31	0:43:33.406	41:43:32.900	1.8884	22.00	-	3.0	1.7	
f2BEB622	0:43:31.104	41:42:03.049	2.9382	21.59	21.55	3.5	1.0	
f2BEB5712	0:43:41.098	41:22:09.529	3.8868	21.15	-	5.5	2.5	
f2BEB5393	0:43:36.168	41:23:08.147	2.2315	21.50	-	2.5	1.0	
f2BEB986	0:43:29.868	41:40:52.399	5.989	22.26	-	2.3	2.0	
f2BEB393	0:43:31.551	41:42:40.693	1.6741	22.11	21.96	0.5	0.4	
f2BEB1806	0:43:04.932	41:38:07.633	2.619, 2.609	21.94	21.72	1.5	0.5	
f2BEB2857	0:43:00.719	41:34:16.919	2.0887	20.79	20.97	3.3	1.9	
f2BEB371	0:43:35.647	41:42:44.426	2.8777	21.44	21.06	2.5	2.5	
f2BEB1878	0:43:03.565	41:37:52.247	5.41	20.56	20.32	6.5	-	2
f2BEB1352	0:42:53.333	41:39:42.250	4.61, 5.86	21.78	21.46	1.8	-	2
f2BEB1227	0:42:46.247	41:40:06.210	3.264, 4.444	22.69	-	1.5	-	2
f2BEB629	0:43:26.095	41:42:01.193	4.2745	20.44	20.09	4.5	4.0	
f2BEB4356	0:42:53.182	41:27:14.506	1.8776	19.92	20.17	5.5	4.0	

¹from Walterbos & Braun (1992)²Eclipse has no bottom, therefore flux depth unreliable**REFERENCES**

- Andersen J., 1991, *A&A Rev.* 3, 91.
Baade W., Swope H.H., *AJ*, 1963, 68, 435.
Berkhuijsen E.M., Humphreys R.M., Ghigo F.D., Zumach W., 1988, *A&AS* 76, 65.
Bond I.A., Abe F., Dodd R.J., Hearnshaw J., Honda M., Jugaku J., Kilmartin P.M., Marles A. et al., 2001, *MNRAS* 327, 868.
Bramich D.M., Horne K., Bond I.A., Street R.A., Collier Cameron A., Hood B., Cooke J., James D., et al., 2005, *MNRAS*, 359, 1096.
Clausen J.V., 2003, *A&A*, 402, 509.
Clausen J.V., 2004, *New Astron. Rev.* 48, Issue 9, 679.
Clementini G., Federici L., Corsi C., Cacciari C., Bellazzini M., Smith H.A., 2001, *ApJ*, 559, L109.
Cole A.A., 1998, *ApJ*, 500, L137.
Fitzpatrick E.L., Ribas I., Guinan E.F., Maloney F.P., Claret A., 2003, *ApJ* 587, 685.
Freedman W.L., Madore B.F., Gibson B.K., Ferrarese L., Kelson D.D., Sakai S., Mould J.R., Kennicutt R.C., et al., 2001, *ApJ*, 553, 47.
Gaposhkin S., 1968, *PASP*, 80, 556.
Guinan E.F., Fitzpatrick E.L., Dewarf L.E., Maloney F.P., Maurone P.A., Ribas I., Pritchard J.D., Bradstreet D.H., 1998, *ApJ*, 509, L21.
Guinan E., 2004, *New Astron. Rev.* 48, Issue 9, 647.
Harries T.J., Hilditch R.W., Howarth I.D., 2003, *MNRAS*, 339, 157.
Hilditch R.W., Howarth I.D., Harries T.J., 2005, *MNRAS*, 357, 304.
Kaluzny J., Stanek K.Z., Krockenberger M., Sasselov D.D., Tonry J.L., Mateo M., 1998, *AJ*, 115, 1016.

Table 5. EBs in Field 3 of the Andromeda Galaxy.

ID	RA (J2000)	DEC (J2000)	P (d)	B_{max}	V_{max}	D_p	D_s	Notes
f3BEB2506	0:43:58.089	41:50:28.572	2.7491	20.53	20.45	8.1	5.6	
f3BEB670	0:45:19.706	41:45:05.364	7.061	20.38	19.41	-	-	2, V5407 DIRECT
f3BEB1265	0:44:50.255	41:51:24.232	1.9428	20.65	20.55	8.4	6.0	
f3BEB1285	0:44:49.119	41:52:52.890	2.6270	19.52	19.52	20	20	
f3BEB2388	0:44:04.561	41:48:52.159	2.6475	20.60	20.17	11	10	
f3BEB1784	0:44:30.461	41:52:04.393	6.2241	20.17	20.73	14	13	
f3BEB750	0:45:20.086	41:45:04.227	1.6041	20.13	20.45	13	10	V4741 DIRECT
f3BEB456	0:45:32.433	41:47:42.806	2.7879	19.90	19.89	18	10	V7393 DIRECT
f3BEB1778	0:44:30.629	41:51:56.121	1.4067	20.46	20.32	3.8	3.8	
f3BEB760	0:45:19.706	41:45:05.364	5.75	19.24	19.41	27	20	DEB,V4636 DIRECT
f3BEB630	0:45:25.503	41:45:04.005	5.010	20.04	19.99	8.5	-	2, V5912 DIRECT
f3BEB1547	0:44:37.084	41:52:25.119	4.768	19.86	19.99	-	9	2
f3BEB251	0:45:38.924	41:47:49.825	1.2772	20.46	20.86	5.5	5.5	
f3BEB2260	0:44:09.540	41:47:04.875	2.7721, 3.129, 3.012	20.77	20.96	4.5	-	2
f3BEB562	0:45:28.366	41:44:24.375	3.080	20.54	20.56	6.0	6.0	V6450 DIRECT
f3BEB580	0:45:28.150	41:49:32.961	4.37, 3.60	20.80	20.76	-	-	2, V6527 DIRECT
f3BEB651	0:45:24.220	41:46:26.850	6.798	20.10	20.28	9	6.5	
f3BEB505	0:45:31.116	41:46:49.598	4.504	21.31	21.47	1.8	1.8	
f3BEB1276	0:44:49.372	41:52:17.821	4.771	20.47	20.39	-	-	2

²Eclipse has no bottom, therefore flux depth unreliable

- Kiss L.L., Bedding T.R., 2005, MNRAS, 358, 883.
 Macri L., 2004, New Ast. Rev., 48, Issue 9, 675.
 Magnier E.A., 1996, A&A Supp., 96, 379.
 McConnachie A.W., Irwin M.J., Ferguson A.M.N., Ibata R.A., Lewis G.F., Tanvir N., 2005, MNRAS 356, 979.
 Mochejska B.J., Kaluzny J., Stanek K.Z., Sasselov D.D., 2001, AJ 122, 1383.
 Mochejska B.J., Macri L.M., Sasselov D.D., Stanek K.Z., Sasselov D.D., 2004, ASPC 310, 41.
 Mould J., Saha A., Hughes S., 2004, ApJS, 154, 623.
 Ribas I., Fitzpatrick E.L., Maloney F.P., Guinan E.F., Udalski A., 2002, ApJ, 574, 771.
 Schwarzenberg-Czerny A., 1989, MNRAS, 241, 153.
 Stellingworth R.F., 1978, ApJ, 224, 953.
 Veltchev T., Nedialkov P., Borisov G., 2004, A&A, 426, 495.
 Waltherbos R.A.M., Braun R., 1992, A&AS, 92, 625.
 Wilson R.E., 2004, New Astron. Rev., 48, Issue 9, 695.

This paper has been typeset from a \TeX / \LaTeX file prepared by the author.

Table 6. EBs in Field 4 of the Andromeda Galaxy.

ID	RA (J2000)	DEC (J2000)	P (d)	B_{max}	V_{max}	D_p	D_s	Notes
f4BEB1695	0:44:27.199	41:36:08.223	4.5186	20.19	20.03			V1266 DIRECT
f4BEB821	0:45:12.519	41:37:26.321	2.3584	19.33	19.29			V7940 DIRECT
f4BEB1157	0:45:05.377	41:33:40.442	1.7699	20.12	20.22			V6846 DIRECT
f4BEB1180	0:45:04.843	41:37:29.350	3.0945	19.25	19.41			V6840 DIRECT
f4BEB1962	0:44:11.074	41:34:08.197	2.9202	19.84	19.84			
f4BEB2294	0:43:53.920	41:36:42.418	6.242	20.89	21.02			
f4BEB246	0:45:26.694	41:41:03.179	2.0833	20.71	20.95			V6024 DIRECT
f4BEB1672	0:44:28.010	41:36:57.330	2.8949	21.62	-			
f4BEB1763	0:44:24.763	41:39:02.422	4.763	19.98	20.04			V888 DIRECT
f4BEB1802	0:44:22.332	41:38:51.216	0.2326	18.68	17.80			V438 DIRECT, Local WUMa
f4BEB74	0:45:37.723	41:43:07.777	1.9302	20.94	20.81			V8420 DIRECT
f4BEB930	0:45:10.294	41:36:47.119	6.0972, 3.049, 5.1395	18.78	18.85			V7628 DIRECT
f4BEB1621	0:44:31.171	41:36:15.288	1.553	20.52	19.61			1
f4BEB1893	0:44:15.941	41:37:29.369	2.7262	21.84	-			
f4BEB1168	0:45:05.200	41:38:46.464	0.91664	20.77	20.71			V1555 DIRECT
f4BEB2290	0:43:54.185	41:37:13.150	3.335	20.65	20.73			
f4BEB920	0:45:10.432	41:36:34.421	6.7657	20.40	20.33			Unusual LC
f4BEB990	0:45:09.190	41:38:41.867	4.4523	20.25	20.36			
f4BEB296	0:45:24.691	41:39:41.341	2.4223	21.61				
f4BEB1617	0:44:31.538	41:37:22.253	4.6471	21.76				
f4BEB1994	0:44:10.634	41:39:49.699	5.4995	21.72				1
f4BEB527	0:45:18.676	41:40:47.040	2.0215	20.61	20.67			
f4BEB1465	0:44:49.047	41:32:59.691	0.95183	21.28	21.26			
f4BEB2006	0:44:10.277	41:39:49.409	2.8143	20.98	20.79			
f4BEB2050	0:44:08.816	41:39:49.889	1.7957	21.33				
f4BEB953	0:45:09.761	41:34:17.287	1.7806	21.59	21.28			
f4BEB698	0:45:14.908	41:40:30.521	2.4350	20.49	20.47			
f4BEB428	0:45:20.771	41:38:27.814	1.9108	21.40	-			
f4BEB453	0:45:20.351	41:41:44.412	1.0791	20.93	21.04			
f4BEB1915	0:44:13.536	41:39:19.126	1.9272	21.02	20.91			

¹Multiple aliases within ± 0.05 d of the quoted period.²Eclipse has no bottom, therefore flux depth unreliable